Proceedings of the 21st ICSMGE, Vienna, Austria, 14 – 19 June 2026. Pistrol, Adam & Schweiger (eds.)
Published by: ÖGG, Austrian Society for Geomechanics, Salzburg, Austria, ISBN 978-3-9503898-4-5
https://doi.org/10.53243/ICSMGE2026-1214

Integrating InSAR and numerical modelling to analyse landslide-bridge interaction

Erica Cernuto, Diana Salciarini, Filippo Ubertini
Department of Civil and Environmental Engineering, University of Perugia, Via Goffredo Duranti, 93, Perugia, 06126, Italy, erica.cernuto@dottorandi.unipg.it

Giorgia Giardina
Department of Geoscience and Engineering, Delft University of Technology, Stevinweg 1, Delft, 2628 CN, The Netherlands

ABSTRACT: Landslides that affect critical infrastructure pose significant challenges in understanding their dynamics and assessing the risks to structures. To address these phenomena, this study adopts a combined approach that integrates InSAR satellite monitoring with three-dimensional numerical modelling to achieve a more comprehensive characterisation than using each method in isolation. InSAR is effective in detecting surface deformations and their temporal evolution over large areas, but it is limited by its one-dimensional Line-of-Sight geometry and its inability to capture deep-seated movements or to simulate the internal evolution of the landslide. Numerical modelling complements these observations by reconstructing displacements along the main direction of movement, defining the trajectory of the landslide, and providing insight into its internal processes. At the same time, InSAR data offer direct observations of surface movements that are essential for validating numerical results. The aim of this work is to combine the two techniques to analyse the landslide-bridge interaction. Although the case study is exemplary, the results have broader applicability and highlight the advantages of the integrated approach. The InSAR analysis revealed predominantly transverse displacements, with a less significant vertical component, consistent with the observed kinematics, enriching traditional observations and improving the understanding of landslide behaviour on a regional scale. Numerical modelling confirmed this pattern and revealed significant displacements in the structural elements of the bridge, with tilting downstream caused by the horizontal thrust of the landslide. It also provided insights into areas lacking satellite coverage, particularly at the toe of the slope. The comparison between observed and simulated displacements increased the reliability of the results and supported the identification of critical areas. The integrated approach improved the ability to monitor and predict landslide impacts, serving as a valuable tool for risk management and infrastructure protection in vulnerable areas, with broad applicability to similar phenomena.

KEYWORDS: InSAR, 3D Numerical Modelling, Landslide-bridge interaction, Combined Approach.

1 INTRODUCTION

Landslides pose an increasing threat to infrastructure such as bridges, with potentially severe impacts on structural stability; however, the complex interaction between landslides and built structures continues to challenge the development of accurate simulation models. One promising approach for assessing infrastructure safety in landslide-prone areas is the integration of surface displacement data, acquired through advanced monitoring techniques like Synthetic Aperture Radar Interferometry (InSAR), with robust numerical modelling.

InSAR enables the monitoring of large-scale surface deformation at relatively low cost and without the need for ground-based instrumentation, making it particularly effective in remote or inaccessible areas (Solari et al., 2020). However, it only measures displacements along the Line of Sight (LOS) between the satellite and the target, providing a one-dimensional projection of movements that occur in three-dimensional space. This can result in underestimation or complete omission of displacements, especially when the dominant movement occurs perpendicular to the LOS (Hu et al., 2014). This limitation is particularly relevant for landslides, which often exhibit dominant horizontal movements (Song et al., 2021). Overcoming this issue requires converting LOS measurements into true three-dimensional components using post-processing techniques. Several methods have been proposed to achieve this (Notti et al., 2014; Brouwer, 2021; Farneti et al. 2023), but no standardised approach has yet been established. Accurate 3D reconstruction also requires that ascending and descending data coincide spatially and temporally, a condition rarely met, making resampling and temporal alignment necessary. For example, Casagli et al. (2009) used a vector-based resampling on a regular grid, while Notti et al. (2014) matched Persistent Scatterer (PS) pairs based on the geometric distance between points in the two orbital geometries. Despite the variety of methods available, it remains challenging to identify a universally effective approach in landslide-prone areas, where environmental factors such as vegetation significantly affect PS availability. While InSAR is effective in surface monitoring, it cannot capture deep-seated movements or simulate landslide evolution, which are crucial aspects that can be addressed by 3D numerical modelling. Combining the two approaches thus improves the understanding of landslide mechanisms and allows for predictions of future deformations (Sun et al., 2023; Meoni et al., 2024).

Understanding the processes governing landslide phenomena through numerical simulations is essential for effective risk management, particularly for infrastructure interacting with slope movements. In this context, 3D modelling, compared to traditional 2D approaches, provides a more comprehensive representation of the morphological and structural characteristics of landslides (Morcioni et al., 2023), enabling accurate simulations of deformation propagation and interactions with the affected infrastructure. These models not only allow the simulation of deformation evolution but can also determine the landslide movement direction and the maximum velocity (Hu et al., 2020). Moreover, they make it possible to reconstruct the landslide trajectory, providing crucial information to identify the most hazardous areas and to analyse slope stability (Gardezi et al., 2021), thereby enhancing the understanding of landslide behaviour. Among numerical approaches, the Finite Element Method (FEM) is particularly effective for modelling non-linear soil behaviour (Pauselli et al., 2022). However, model calibration requires accurate input data, which are often limited or based on localised investigations (Rainders et al., 2022). In this context, InSAR contributes significant value, aiding calibration and validation. When combined with ground-based measurements, it also supports geological interpretation and understanding of

landslide geometry and kinematics (Tofani et al., 2013). Therefore, integrating satellite data and numerical modelling represents a promising solution for achieving more accurate and reliable predictions.

This study presents an integrated approach that combines InSAR data and numerical modelling to investigate the interaction between a landslide and a bridge. The approach estimates two-dimensional displacement components from satellite observations and simulates the landslide–structure interaction through a calibrated 3D model. This integration supports identifying critical areas and provides a valuable tool for assessing landslide-related infrastructure risks. It should be noted that the data used derive from past investigations and do not necessarily reflect current conditions . It is clarified that this study does not aim to investigate the current stability conditions of the system or the landslide phenomenon, it is used to demonstrate the applicability of the approach.

2 CASE STUDY

The study area is located in a municipality in the Parma province (Emilia-Romagna, Italy), featuring complex geology and moderately inclined slopes (10°–15°), within a geomorphologically unstable setting typical of the Northern Apennines, as highlighted in the IFFI inventory (Figure 1Figure 1Figure 1a).

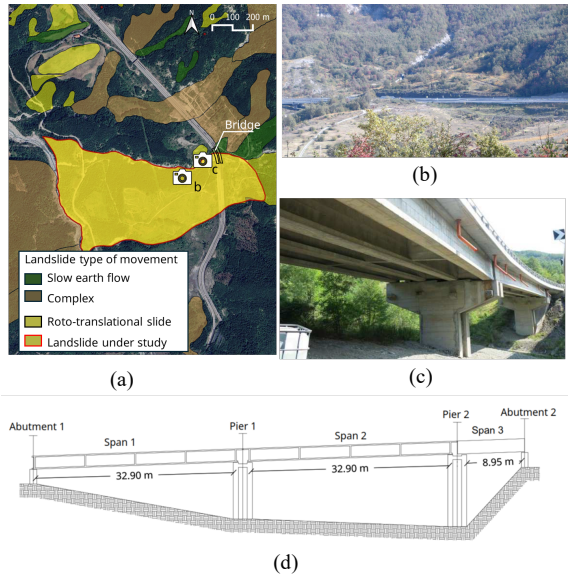

Figure 1. (a) Extract from the IFFI inventory; (b) overview of the unstable slope in proximity to the bridge; (c) view of the bridge; (d) longitudinal section of the bridge.

The analysed phenomenon is a roto-translational landslide that directly interferes with a motorway bridge. Geologically, the landslide develops across a tectonic contact between Scabiazza Sandstones (upstream) and Blocky Clays of the Casanova Complex (downstream), with interbedded Palombini Shales. This stratigraphic setting favours slope instability.

A comprehensive field investigation campaign allowed for detailed characterisation of landslide geometry and kinematics. Inclinometers, piezometers, and topographic targets were installed and complemented by laboratory tests on borehole samples. Inclinometers identified a sliding surface at about 80 m depth, with average displacements of 6.5 cm/year, consistent with topographic monitoring between 1975 and 2015. In 2015, new inclinometers were installed, recording active movements of 4–6 mm/month at depths of 37–38 m (for further details see Cernuto et al. 2025). Grain size analyses on six samples revealed a fine silty-clayey matrix. The presence of a shallow water table further reduces slope stability.

The landslide extends approximately 1000 m in length and 300 m in width, with an average slope of 10° and a maximum depth of 80 m. The interfered bridge analysed in this study consists of three spans (Figure 1Figure 1Figure 1c,d): two main spans of 32.9 m with simply supported post-tensioned precast beams, and a shorter end span (8.95 m) with a reinforced concrete slab. The foundations of the piers and abutments consist of large-diameter caissons: approximately 6 m for the abutments and 7 m for the piers. All caissons are lined with 50 cm thick concrete and reach a depth of about 12 m.

3 METHODOLOGICAL APPROACH

The proposed approach integrates InSAR monitoring and numerical modelling to analyse the interaction between the landslide and the bridge. InSAR allows large-scale monitoring of surface displacements and their temporal evolution, but reconstructing the full 3D displacement vector from the Line of Sight (LOS) component is highly uncertain and requires additional input. Numerical modelling simulates the landslide's 3D behaviour and defines the main movement direction based on slope topography, following the steepest descent path. However, it does not offer a direct reference to determine whether the estimated displacements are consistent with the actual behaviour of the phenomenon. In this context, satellite data serve as essential observational support to compare numerical estimates with real-world observations. Integrating both methods improves the overall reliability and consistency of the analysis.

3.1.1 *Numerical Modelling*

The numerical modelling was performed using the finite element software Plaxis 3D (Brinkgreve et al., 2016). The soil topography was defined from contour lines with a 5 m interval to represent the actual site morphology accurately. The soil was modelled as a homogeneous, non-stratified volume composed of silty-clayey material, identified based on grain size analyses. The landslide was reproduced in the model according to the dimensions provided in Section 2 and is characterised by a roto-translational movement along a sliding surface (Figure 2a).

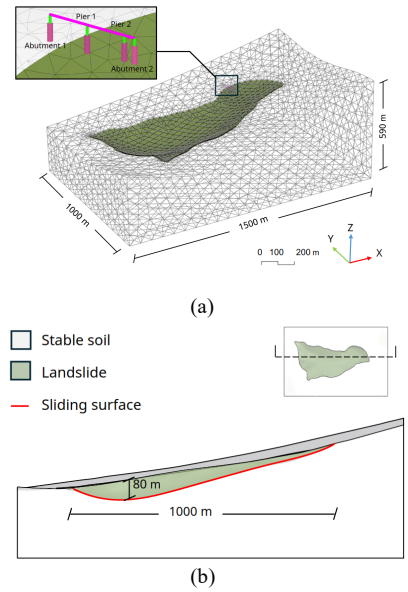

Figure 2. (a) Three-dimensional view of the model with the bridge integrated in Plaxis 3D; (b) longitudinal cross-section of the three-dimensional soil.

The model includes two main volumes (Figure 2b): stable soil and landslide. These materials are associated with the same physical and mechanical properties, except for strength parameters (cohesion and friction angle), which were calibrated through a back-analysis using an iterative approach. For the stable soil, values of c′=30 kPa and φ′=35° were adopted, while for the landslide volume, c′=28 kPa and φ′=30°. The sliding surface was modelled through a specific interface with residual parameters (c′=1 kPa, φ′=18°). These parameters were initially defined from geotechnical literature (Terzaghi et al., 1996) and then refined through a parametric study to suit the site's specific conditions. Specifically, the values of cohesion and friction angle were adjusted to ensure that the simulated instability mechanism aligned consistently with the observations made on site. The Hardening Soil constitutive model was assigned to all materials, as it simulates the non-linear behaviour of soil and the variation in stiffness as a function of strain level. Stiffness was defined using three parameters: the secant modulus E_{50}^{ref}, the oedometer modulus E_{oed}^{ref}, and the unloading/reloading modulus E_{ur}^{ref}, estimated based on the geotechnical characteristics of the site and empirical correlations from literature (Table 1. Strength parameters adopted for stable soil, landslide volume and sliding surface. Additionally, the model includes parameter *m*, which accounts for stiffness dependency on effective stress, adopted following the values proposed by Janbu (1963) and Wu and Tung (2020).

Table 1. Strength parameters adopted for stable soil, landslide volume and sliding surface.

Parameter	Value	Unit
Secant stiffness ($\mathbf{E_{50}^{ref}}$)	30.00e^3	kN/m^2
Tangent stiffness ($\mathbf{E_{oed}^{ref}}$)	36.01e^3	kN/m^2
Unloading/reloading stiffness ($\mathbf{E_{ur}^{ref}}$)	110.80e^3	kN/m^2
Power for stiffness dependency on stress level (**m**)	0.5	-

After defining the soil geometry and properties, the bridge structure was modelled using the geometric information provided in Section 2 (Figure 2a). Since the focus is on the soil–foundation interaction, simplifications were applied to the superstructure: the piers were modelled as linear elastic beams and the deck as a simply supported beam. The presence of groundwater was also considered by introducing a piezometric surface 2.5 m below ground level. The analysis was carried out through progressive phases: the initial stress state was first established, followed by a plastic phase for elasto-plastic deformation, and concluded with a global stability analysis based on the strength reduction method.

3.1.2 *InSAR analysis*

The satellite analysis was conducted using InSAR data from Sentinel-1, with a temporal resolution of six days, made available by the Copernicus program's European Ground Motion Service (EGMS). The EGMS provides three levels of interferometric products: Basic, Calibrated, and Ortho. In this study, the Calibrated product (Level 2B) was selected, as it provides deformation velocities along the Line of Sight (LOS) referenced to a terrestrial reference system, through calibration with GNSS data, and is available in both ascending and descending geometries. Although the Ortho product (Level 3) directly provides the vertical and horizontal displacement components, it was not used due to its low spatial resolution (100 m grid), which significantly reduces the number of available points within the area of interest. Furthermore, the displacement components are expressed in the ETRS89-LAEA reference system (East, North, Vertical), which is not always optimal for representing the orientation of the deformation phenomena. A local reference system (L, T, V), aligned with the direction of the phenomenon, was adopted to ensure a more coherent representation of actual ground movement.

The analysed datasets cover 2018–2022 and include ascending (06/01/2018–23/12/2022) and descending (05/01/2018–22/12/2022) acquisitions. Interferometric techniques detect only the displacement component along the LOS, which may lead to underestimation when significant horizontal displacements are involved. To overcome this limitation, post-processing was performed to reconstruct the actual displacement components. This operation requires that the PS from both geometries are spatially and temporally matched, a condition that is rarely met and therefore addressed through spatial and temporal interpolation. The proposed methodology is organised into two main phases.

The first phase included the resampling of the data, performed using a regular grid with 25 m square cells (Figure 1a), designed according to the density of PS in the ascending and descending geometries. This size ensured a sufficient number of PS in each cell, considering the heterogeneous distribution of the data, with lower density in the landslide area (covered by vegetation) compared to the bridge's surroundings. Due to the limited availability of dual-geometry data downstream, the analysis focused on the upstream section, where the interaction with the infrastructure occurs.

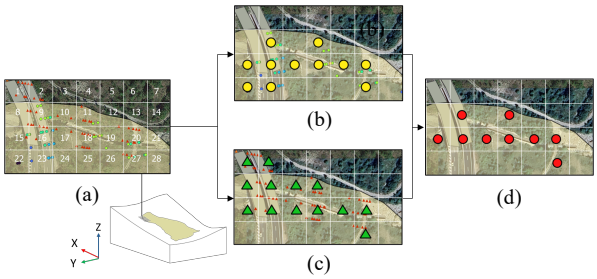

Figure 3. Combination schema of ascending and descending datasets: (a) resampling grid, (b) ascending synthetic PS, (c) descending synthetic PS, (d) combined synthetic PS.

The grid configuration was chosen after comparing different methods, such as that by Notti et al (2010), which uses pairing via a 7 m buffer, and that by Casagli et. al (2009) with a 50 m mesh. Both approaches showed limitations due to outliers caused by vegetation, whose signal is influenced by wind and seasonal variations. Therefore, adopting a finer mesh allowed us to overcome these issues. Once the grid was defined, a synthetic PS was computed at the centroid of each cell for both orbital geometries (Figure 3b and c), as the average LOS value of the PS within the cell over all acquisition dates. Since ascending and descending acquisitions are not simultaneous, post-processing was applied to align the datasets, considering only the common time interval (06/01/2018–22/12/2022). The time series were interpolated to estimate missing values, and only synthetic PS present in both geometries were combined (Figure 3d), producing a consistent time series with LOS values from both geometries.

The second phase focused on estimating the actual displacement components from the deformation measured along the satellite's Line of Sight (LOS), by adapting and combining the approaches proposed by Brouwer et al. (2021) and Farneti et al. (2023), suitably modified for the present case study. In the global reference system (E, N, V), the actual displacement *d* is estimated from the measured LOS displacement d_{LOS} (Figure 4a) using the following equation:

$$d = \frac{d_{LOS}}{u_d \bullet u_{LOS}} = \frac{d_{LOS}}{\cos\theta \cos w + \sin\theta \sin w \cos(\alpha+\phi)} \quad (1)$$

In this expression, u_d and u_{LOS} are unit vectors defining the directions of the actual displacement and LOS in the global coordinate system. The parameter θ represents the incidence angle between the LOS and the vertical direction, while α is the angle between the horizontal projection of the LOS and the East axis. The direction of the actual displacement vector is described by the vertical and horizontal angles ω and φ. Despite its widespread use, the global reference system is not always the most suitable for representing ground deformation, as the primary displacement directions may not align with East, North, or Vertical. To obtain a more meaningful representation of the actual motion, a local reference system (L, T, V) was adopted (Figure 4b). This system is fixed to the deformation phenomenon, with the T-axis aligned with the main direction of movement, derived from numerical modelling and corresponding to the direction of maximum slope in the landslide area.

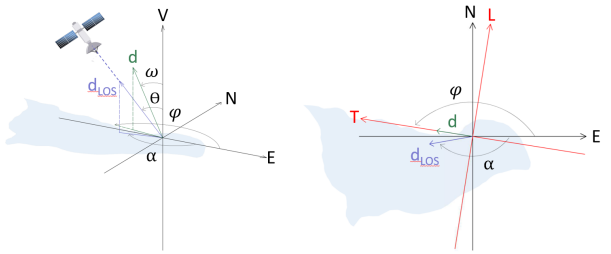

Figure 4. Representation of: (a) global reference system (N, E, V); (b) local reference system fixed to the deformation phenomenon (L, T, V).

Assuming that the actual displacement occurs in each of these directions (L, T, V), and that no other movement contributes to the LOS measurement at a given time, the components of the actual displacement can be derived as follows:

$$d_L = \frac{d_{LOS}}{\sin\theta \sin(\alpha+\phi')}\ ;\ d_T = \frac{d_{LOS}}{\sin\theta \cos(\alpha+\phi')}\ ;\ d_V = \frac{d_{LOS}}{\cos\theta} \quad (2)$$

Accordingly, the LOS measurement can be expressed as a linear combination of the three real displacement components:

$$d_{LOS} = d_L \sin\theta \sin(\alpha+\phi') + d_T \sin\theta \cos(\alpha+\phi') + d_V \cos\theta \quad (3)$$

In general, estimating the complete 3D displacement vector (d_L, d_T, d_V) would require at least three independent LOS geometries, spatially and temporally coincident. However, since only two LOS measurements (ascending and descending) are available, the system is underdetermined:

$$d_{LOS} = Ad \quad (4)$$

where:

$$d_{LOS} = \begin{Bmatrix} d_A \\ d_D \end{Bmatrix},$$

$$A = \begin{bmatrix} \sin\theta_A \sin(\alpha_A+\phi') & \sin\theta_A \cos(\alpha_A+\phi') & \cos\theta_A \\ \sin\theta_D \sin(\alpha_D+\phi') & \sin\theta_D \cos(\alpha_D+\phi') & \cos\theta_D \end{bmatrix}$$

$$d = \begin{Bmatrix} d_L \\ d_T \\ d_V \end{Bmatrix}$$

To solve this system, an additional assumption is introduced: the absence of longitudinal displacement (d_L=0). This assumption is supported by the nature of gravitational landslides, where movement predominantly follows the direction of maximum slope (T-axis in the local system), and deformation parallel to contour lines is generally negligible. Under this assumption, the system becomes determined and can be written as:

$$\hat{d} = B^{-1} d_{LOS} \quad (5)$$

$$\hat{d} = \begin{Bmatrix} d_T \\ d_V \end{Bmatrix}, \quad B = \begin{bmatrix} \sin\theta_A \cos(\alpha_A+\phi') & \cos\theta_A \\ \sin\theta_D \cos(\alpha_D+\phi') & \cos\theta_D \end{bmatrix}$$

Here, $\hat{d}$ denotes the estimated components of the actual displacement in the transverse and vertical directions, and matrix B is obtained from A by removing the column associated with the assumed null component. This procedure enables the transformation of the ascending and descending LOS measurements into a two-dimensional displacement vector aligned with the kinematics of the landslide.

4 RESULTS

Numerical modelling enabled the analysis of both the slope response and the deformations induced on the bridge, providing a comprehensive view of the final equilibrium configuration of the system under stationary conditions. The results reveal a non-uniform spatial distribution of total displacements |u| within the landslide volume (Figure 5): maximum values of approximately 14 cm are observed in the downstream area, while in the upstream portion, displacements are more limited (around 10 cm). Near the bridge, values decrease further to about 4 cm, indicating a mitigating effect due to the presence of the structure. Analysis of the displacement components shows a predominance of the horizontal components, with u_x up to -3 cm and u_y up to 2.5 cm, while the vertical component is negligible. This behaviour is consistent with the landslide kinematics, characterised by predominantly horizontal movements.

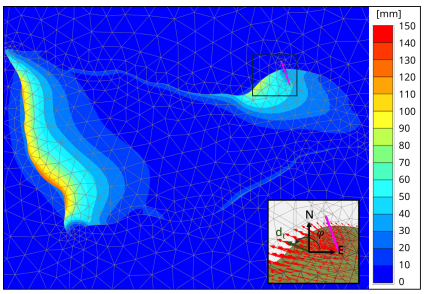

Figure 5. Top view of total displacement contours (|u|); red arrows (bottom right) indicate main landslide movement direction in the NE plane

Regarding the response of the structural elements to the landslide movement, the bridge piers and their foundations were analysed. Displacements were evaluated at the nodes located at the base of each pier (top of the foundation structure) and the pier heads (deck level). The results (Figure 6) show significant displacements for Pier 2 and Abutment 2, located within the landslide volume, mainly at their bases and aligned with the direction of the landslide. Abutment 1, positioned outside the affected area, shows minimal displacements in the opposite direction. Pier 1, located in an intermediate position between the stable zone and the active landslide body, shows greater displacements than Abutment 1, indicating increasing interaction with the landslide movement. Overall, elements located within or near the landslide volume are more affected by the horizontal thrust generated by the moving mass. The limit equilibrium analysis yielded a global safety factor of 1.2274, suggesting a condition close to the limit of stability that requires ongoing monitoring. Furthermore, when observing the

deformation mechanism of the bridge (Figure 7), it is evident that the structure located within the landslide area is dragged in the direction of the landslide movement. This dragging effect is primarily caused by the horizontal thrust exerted by the moving landslide mass on the bridge foundations, resulting in a deformation consistent with the prevailing direction of the landslide kinematics.

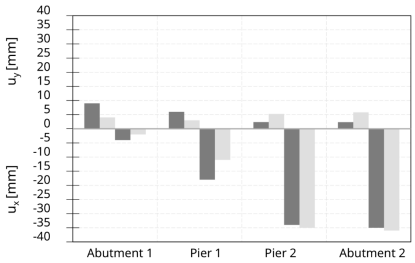

Figure 6. Graphical representation of horizontal displacements recorded at the top and base of the piers and abutments.

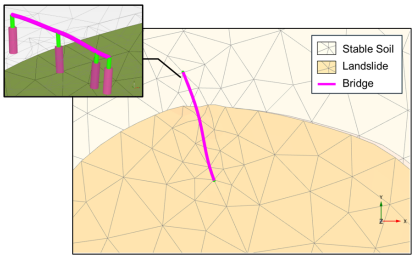

Figure 7. Representation of the bridge deformation mechanism.

As for the satellite data, the post-processing involved combining LOS measurements from ascending and descending geometries. A 25 m regular grid was used for resampling to ensure spatial and temporal correspondence, enabling the definition of a single LOS displacement time series for each synthetic point in both orbits (Figure 8a, b).

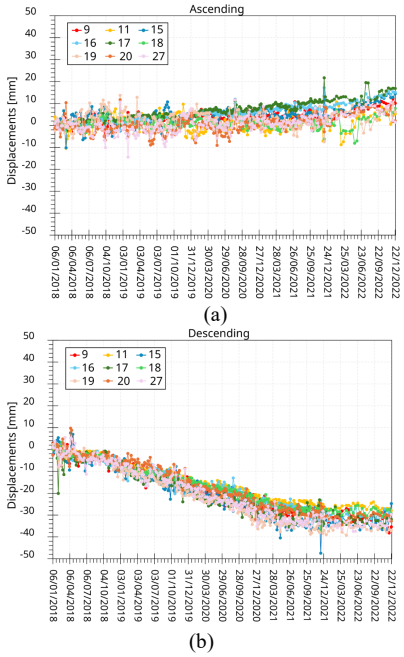

Figure 8. Time evolution of displacements along the LOS in ascending and descending geometries for synthetic PS defined on a 25 m grid

Within the landslide volume, LOS time series show opposite signs: positive in the ascending geometry (motion toward the satellite looking west) and negative in the descending geometry (motion away from the satellite looking east). This behaviour is consistent with the landslide kinematics under investigation, typical of phenomena characterised by predominantly horizontal deformation components. The combined observation confirms a coherent westward movement, in line with the prevailing direction identified through numerical modelling.

Combining the two geometries and assuming zero longitudinal displacement, the actual displacement components were estimated in a local reference system aligned with the landslide direction. Results reveal a progressive increase in the transverse component (d_T) up to ~40 mm (Figure 9a), and a vertical lowering (d_V) of about –20 mm (Figure 9b), confirming a mainly horizontal dynamic with a non-negligible vertical component.

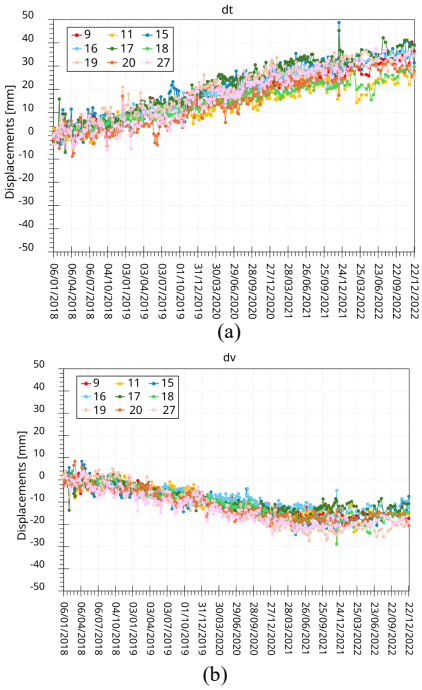

Figure 9. Time evolution of the two components of the actual displacement of the identified synthetic PS: (a) transverse (d_T) and (b) vertical (d_V).

To evaluate the reliability of the results, a comparison was carried out between the displacements estimated from InSAR data and those recorded by traditional monitoring. Although ground-based measurements cover a broader portion of the landslide (including downstream sectors with limited satellite coverage), the comparison focused on topographic targets 2, 5, 7, and 8, located near the synthetic PS (Figure 10).

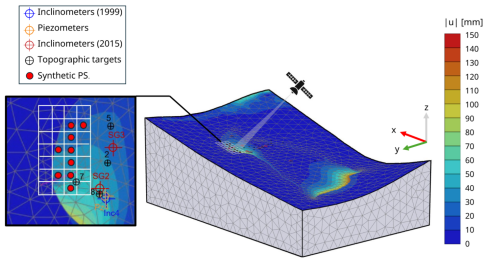

Figure 10. Spatial comparison of total displacements from numerical modelling, instrumental monitoring targets, and synthetic PS derived through 25 m grid resampling.

Between 1975 and 1999, these targets showed movements of about 1.05 m (4 cm/year), decreasing to 0.26 m (2 cm/year) between 2004 and 2015. InSAR data for the 2018–2022 period confirm this deceleration trend, with a maximum displacement of 40 mm (1 cm/year). This evolution reflects a gradual reduction in activity, consistent with the long-term behaviour of the landslide under stable external conditions. In addition, a

qualitative comparison was made between the spatial distribution of displacements derived from InSAR and those predicted by numerical modelling. While the two approaches refer to different temporal contexts, with InSAR data capturing transient displacements and the numerical model simulating the final equilibrium, the results are consistent. The upper portion of the landslide, where synthetic PS are available, shows consistent movement patterns between the two datasets. Although InSAR data are lacking in the downstream area, numerical results suggest greater displacements in that sector, supporting the overall consistency of the two analyses.

5 CONCLUSION

The integrated approach proposed in this study, which combines InSAR satellite interferometry and three-dimensional numerical modelling, proved highly effective in analysing the interaction between landslides and infrastructure. The methodology demonstrated that integrating satellite-based monitoring with numerical models provides complementary and more detailed insights than either method used independently. InSAR analysis offered a comprehensive overview of surface displacements; however, its one-dimensional nature along the sensor's line of sight limits its ability to characterise the phenomenon in three dimensions fully. In this context, numerical modelling emerged as a valuable complementary tool, allowing for estimating actual displacement components and identifying the main direction of movement. The satellite results confirmed predominantly transverse movements, with a less pronounced vertical component, consistent with the observed landslide kinematics. InSAR data expanded the information provided by traditional monitoring, which was essential for building the numerical model, by offering more recent displacement measurements and contributing to a broader and more detailed representation of landslide behaviour. Numerical modelling enabled a detailed investigation of the interaction between the landslide and the bridge, highlighting a spatially variable displacement pattern. Larger displacements were observed in the downstream section, gradually decreasing near the bridge, suggesting a possible mitigating effect exerted by the structure. Despite the difference between a steady-state numerical simulation and satellite-based monitoring over four years, the qualitative comparison between the two methodologies showed consistency in the upper landslide area, where critical zones identified by the model aligned with satellite data. In the lower portion, where InSAR coverage is lacking, the model still indicated significant displacements. Therefore, integrating the two approaches improved the interpretation of ground deformations and the estimation of displacement components, providing valuable insights for stability assessment and risk management.

6 ACKNOWLEDGEMENTS

This study was supported by FABRE – "Research consortium for the evaluation and monitoring of bridges, viaducts and other structures" (www.consorziofabre.it/en) within the activities of the FABRE-ANAS and FABRE-ASTM 2021-2026 research programs. Any opinion expressed in the paper does not necessarily reflect the view of the funder. Additionally, this research was supported by the project "Methodological Approaches for RIsk assessment in the framework of landslide bridge IntEraction (MARIE)". The authors would also like to thank ASTM for sharing the data used in this study; the views expressed in the paper are those of the authors and do not necessarily represent those of ASTM. This publication is also part of the Vidi project InStruct, project number 18912, financed by the Dutch Research Council (NWO).

7 REFERENCES

Brinkgreve, R., Kumarswamy, S., Swolfs, W., Waterman, D., Chesaru, A., Bonnier, P., et al., 2016. *Plaxis 2016*. Delft, the Netherlands: PLAXIS bv.

Brouwer, W., 2021. *An analysis of the InSAR displacement vector decomposition*. MSc Thesis. Delft University of Technology.

Casagli, N., Proietti, C., Righini, G., Cigna, F., Pancioli, V., Colombo, A., Poggi, F., Cantone, P., Galluccio, F., Colombo, D., Ferretti, A., Minati, F., Ciccodemarco, S., Rutigliano, S., Ciminelli, M.G. and Costabile, S., 2009. *Piano straordinario di telerilevamento ambientale. Linee guida per l'analisi dei dati interferometrici satellitari in aree soggette a dissesti idrogeologici*.

Cernuto, E., Salciarini, D., Ubertini, F., Giardina, G. 2025. Landslide-Bridge Interaction: A combined approach based on InSAR data and numerical modelling. *International Journal of Disaster Risk Reduction*, 105568.

Farneti, E., Cavalagli, N., Costantini, M., Trillo, F., Minati, F., Venanzi, I. and Ubertini, F., 2023. A method for structural monitoring of multispan bridges using satellite InSAR data with uncertainty quantification and its pre-collapse application to the Albiano-Magra Bridge in Italy. *Struct Health Monit*, 22(1), pp.353–371.

Gardezi, H., Bilal, M., Cheng, Q., Xing, A., Zhuang, Y., and Masood, T., 2021. A comparative analysis of attabad landslide on january 4, 2010, using two numerical models. *Natural Hazards*, 107:519–538

Hu, J., Li, Z.W., Ding, X.L., Zhu, J.J., Zhang, L. and Sun, Q., 2014. Resolving three-dimensional surface displacements from InSAR measurements: a review. *Earth-Sci Rev*, 133, pp.1–17.

Hu, Y. X., Yu, Z. Y., & Zhou, J. W., 2020. Numerical simulation of landslide-generated waves during the 11 October 2018 Baige landslide at the Jinsha River. *Landslides*, *17*(10), 2317-2328.

Janbu, N., 1963. Soil compressibility as determined by oedometer and triaxial tests. In: *Proc. of the European Conference on Soil Mechanics and Foundation Engineering*. Wiesbaden, 1963. Volume 1, pp.19–25.

Meoni, A., Ierimonti, L., Farneti, E., Castellani, M., Filippucci, F., Natali, A., Celati, S., Scozzese, F., Morici, M., Cavalagli, N., Venanzi, I., Agrawal, A.K., Dall'Asta, A., Salvatore, W. and Ubertini, F., 2024. A new methodology for the diagnosis and monitoring of bridges under slow deformation phenomena. *1*(1), pp. 1-13.

Morcioni, A., Apuani, T. and Cecinato, F., 2023. Piuro Landslide: 3D hydromechanical numerical modelling of the 1618 event. *Geosciences*, 13(2), p.49.

Notti, D., Herrera, G., Bianchini, S., Meisina, C., García-Davalillo, J.C. and Zucca, F., 2014. A methodology for improving landslide PSI data analysis. *Int J Remote Sens*, 35(6), pp.2186–2214.

Pauselli, D., Salciarini, D. and Ubertini, F., 2022. Three-dimensional modeling of soil-structure interaction for a bridge founded on caissons under seismic conditions. *Appl Sci*, 12(21), p.10904.

Reinders, K.J., Giardina, G., Zurfluh, F., Ryser, J. and Hanssen, R.F., 2022. Proving compliance of satellite InSAR technology with geotechnical design codes. *Transp Geotech* 33, p.100722.

Solari, L., Del Soldato, M., Raspini, F., Barra, A., Bianchini, S., Confuorto, P., Casagli, N. and Crosetto, M., 2020. Review of satellite interferometry for landslide detection in Italy. *Remote Sens*, 12(8), p.1351.

Song, C., Yu, C., Li, Z., Pazzi, V., Del Soldato, M., Cruz, A. and Utili, S., 2021. Landslide geometry and activity in Villa de la Independencia (Bolivia) revealed by InSAR and seismic noise measurements. *Landslides*, 18(8), pp.2721–2737.

Sun, D., Deng, W., Yang, T., Li, J. and Zhao, Y., 2023. A case study integrating numerical simulation and InSAR monitoring to analyze bedding-controlled landslide in Nanfen Open-Pit Mine. *Sustainability*, 15(14), p.11158.

Terzaghi, K., Peck, R.B. and Mesri, G., 1996. *Soil mechanics in engineering practice*. 3rd ed. New York: John Wiley & Sons.

Tofani, V., Raspini, F., Catani, F. and Casagli, N., 2013. Persistent Scatterer Interferometry (PSI) technique for landslide characterization and monitoring. *Remote Sens*, 5(3), pp.1045–1065.

Wu, J.T. and Tung, S.C.-Y., 2020. Determination of model parameters for the hardening soil model. *Transp Infrastruct Geotech*, 7(1), pp.55–68.